Auger decay calculations with core-hole excited-state molecular-dynamics simulations of water

Osamu Takahashi[a)]
Department of Chemistry, Hiroshima University, Higashi-Hiroshima 739-8526, Japan

Michael Odelius
FYSIKUM, AlbaNova University Center, Stockholm University, S-10691 Stockholm, Sweden

Dennis Nordlund and Anders Nilsson
Stanford Synchrotron Radiation Laboratory, P.O. Box 20450, Stanford, California 94309, and FYSIKUM, AlbaNova University Center, Stockholm University, S-10691 Stockholm, Sweden

Hendrik Bluhm
Chemical Sciences Division, Lawrence Berkeley National Laboratory, Berkeley, California 97420

Lars G. M. Pettersson
FYSIKUM, AlbaNova University Center, Stockholm University, S-10691 Stockholm, Sweden

(Received 9 August 2005; accepted 20 December 2005; published online 10 February 2006)

We report a new theoretical procedure for calculating Auger decay transition rates including effects of core-hole excited-state dynamics. Our procedure was applied to the normal and first resonant Auger processes of gas-phase water and compared to high-resolution experiments. In the normal Auger decay, calculated Auger spectra were found to be insensitive to the dynamics, while the repulsive character of the first resonant core-excited state makes the first resonantly excited Auger decay spectra depend strongly on the dynamics. The ultrafast dissociation of water upon $O(1s) \rightarrow 4a_1$ excitation was analyzed and found to be very sensitive to initial vibrational distortions in the ground state which furthermore affect the excitation energy. Our calculated spectra reproduce the experimental Auger spectra except for the Franck-Condon vibrational structure which is not included in the procedure. We found that the Auger decay of OH and O fragments contributes to the total intensity, and that the contribution from these fragments increases with increasing excitation energy. © *2006 American Institute of Physics*. [DOI: 10.1063/1.2166234]

I. INTRODUCTION

The Auger decay[1,2] is one of the deexcitation processes in atoms and molecules after core excitation; the core-excited species are highly unstable and decay processes follow rapidly. The Auger decay processes are classified based on the excitation energy as "normal" or "resonant" Auger decay for the autoionization of a state created through, respectively, ionization of an inner-shell electron and through resonant excitation of an inner-shell electron to an unoccupied valence orbital. Depending on the potential-energy surface of the excited state the molecule may undergo dynamics during the core-hole lifetime, which depends on the specific element and is in the range of femtoseconds for the second-row atoms. Even if the core-excited state is dissociative, the Auger decay transition in most cases takes place before bond scission. For some special cases, however, the repulsive character of the potential-energy surface in the core-excited state can induce bond scission within the core-hole lifetime; this is usually referred to as ultrafast dissociation. Ultrafast dissociation upon resonant core-excitation into dissociative states has indeed been observed by several authors through effects on the subsequent Auger decay[3–7] and x-ray emission.[8–10] Examples include a number of molecules such as HBr,[3] HCl,[4,5] and water.[6,7,11,12] In the case of water, core excitation into the antibonding $4a_1$ orbital induces ultrafast proton dynamics, seen as a signature of OH+H fragments in the Auger spectra.[7] Hjelte *et al.* used a simplified model for the interpretation of the spectra in which the final state consisted of a distribution of intact H_2O and OH+H fragments.[7] Ultrafast core-excited state dynamics have been observed also in condensed phase by Auger electron-photoion coincidence experiments[13] and x-ray emission spectroscopy.[8,9] Hydrogen bonding plays a significant role in promoting ultrafast dissociation even for core ionization.[8] The applicability of the experimental techniques to condensed phase calls for a development of theoretical tools that can treat complex systems.

Theoretical procedures to calculate Auger decay probabilities for atoms and molecules have been developed by several groups. Two kinds of models, two-step and one-step, have been proposed to describe the Auger decay process. The two-step model treats the absorption and decay processes separately and has been applied to calculate the decay probability from a core-excited state with a fixed geometry. High levels of calculation taking into account electron correlation through configuration interaction[14–21] (CI) or by density-functional theory[22–24] (DFT) have been performed to con-

[a)]Electronic mail: shu@hiroshima-u.ac.jp

struct theoretical Auger spectra in recent years. The energy distribution of the Auger final states can be determined through advanced *ab initio* techniques based on extended configuration spaces. Most applications have used one-center models to calculate the molecular Auger spectra. Very recently, Mitani *et al.* have developed a procedure to calculate theoretical molecular Auger spectra based on electron population analysis.[21] Although the above procedures have been applied to various systems from small molecules to polymers, the dynamical effects of nuclear motion on the Auger spectra have not been considered so far.

A different type of theoretical approach is represented by the one-step model based on the scattering theory under the so-called Auger resonant Raman conditions developed in the last decade,[25–33] which treat the absorption and decay processes simultaneously. An Auger resonant Raman scattering based on time-dependent wave-packet propagation has been developed and applied to the decay process for some diatomic molecules. Furthermore, Tanaka *et al.* showed the dynamical effect in the Auger decay process for BF_3 using a model potential.[34] Actually these procedures have succeeded to describe the experimental spectra, but are too complicated to apply to general polyatomic molecular systems except for highly symmetric molecules such as BF_3.

In the present study, a theoretical procedure is introduced for the normal and resonant Auger spectra based on *ab initio* core-hole excited-state molecular-dynamics (CHES MD) simulations eliminating the need for a predetermined potential-energy surface but restricting the dynamics to classical. A quantum dynamical treatment in terms of a precalculated potential-energy surface necessarily involves a reduction of dimensionality for complex systems, which we can avoid in classical (Newtonian) dynamics simulations. Our procedure represents the first application within the two-step framework to a polyatomic molecule and is here applied to the normal and first resonant Auger spectra of gas-phase water.

II. CALCULATIONAL PROCEDURE

A. DFT calculations

The detailed computational procedure of the DFT part has already been described elsewhere.[35,36] In short, in order to determine the absolute energy position of the excited states, normal ΔKohn-Sham (ΔKS) calculations were performed to compute the ionization energy (IP) including a full relaxation of the core hole. The resonantly excited states were variationally determined with maintained orthogonality between the excited states through the following procedure: The first excited state was obtained by fixing the occupation of the core spin-orbital to zero and placing the excited electron in the first unoccupied orbital. A full relaxation with this constraint leads to a state that is near orthogonal to the ground state due to the $1s^{-1}$ configuration. The next state was then obtained by removing the variationally determined excited orbital from the variational space and occupying the next level. This procedure gives a variational lower bound to the energy and guarantees orthogonality between the excited states since all remaining orbitals now have to be orthogonal to the successively defined and eliminated levels.[36]

In order to estimate absolute excitation energies more accurately, relativistic and functional corrections were added to the excitation energy.[37] Relativistic effects on the IP of 0.33 eV for the O edge and functional corrections to the energy of −0.43 eV were added, where the latter value was determined by the difference between experimental and computational values of the core-ionization energy of water in the gas phase. In order to obtain an improved representation of the relaxation effects in the inner orbitals, the ionized center was described using the IGLO-III basis of Kutzelnigg *et al.*,[38] while a (311/1) basis set was used for the hydrogen atom. The auxiliary basis sets were (3,1;3,1) for hydrogen and (5,2;5,2) for the oxygen atom, where the nomenclature $[N_C(s),N_C(spd);N_{XC}(s),N_{XC}(spd)]$ indicates the number of *s*- and *spd*-type functions used to fit the Coulomb and exchange-correlation potentials, respectively. A gradient-corrected exchange and correlation functionals due to Perdew and Wang were applied in the present study.[39,40] The calculations have been performed using the STOBE-DEMON program.[41]

B. Core-hole excited-state molecular dynamics

In order to consider dynamical effects in the core-excited state, CHES MD simulations were performed.[8] Three types of sampling for the initial states were applied: The first uses the ground-state equilibrium geometry with initial velocities for each atom set to zero. The second samples 60 points from MD simulations of the ground state at room temperature to include vibrational effects in the ground state. The initial velocities for each atom were set to correspond to one of the ground-state normal modes. The third approach to the sampling of initial conditions was used in the simulations of ultrafast dissociation where specific conditions leading to ultrafast dissociation had to be found. As is well known, the $O(1s) \rightarrow 4a_1$ excitation is excited vibrationally due to the differences in the potential-energy surfaces. The ground-state vibrational wave functions furthermore give the probability of finding a particular distortion. Due to the difference in potential-energy surfaces between the ground and excited states the vertical excitation energy required to reach the excited state will not be the same over the full distribution of ground-state structures given by the lowest vibrational wave functions in the ground state. In order to determine the resulting excitation energy over the full geometrical space spanned by the initial-state vibrations several hundred initial structures differing from the ground-state equilibrium geometry through various distortions were sampled. The initial velocities for each atom in these starting geometries were set to zero.

The time step in all CHES MD simulations was set to 1 fs. Although the time step of this study may seem too long in a MD simulation involving proton dynamics, tests with shorter time steps indicate that the induced numerical errors were very small over the 20 fs simulated. We furthermore confirmed that this time step was sufficient for the required resolution of the spectra from experiment. The Verlet inte-

grator was applied to solve the classical equations of motion and the trajectory calculations were propagated for 20 fs, which is sufficiently long for our objective since the short core-hole lifetime, on the order of a few femtoseconds, for the second-row elements ensures that most core-excited states will have decayed within this time.

C. Auger decay calculations

The detailed computational procedure of Auger decay spectra has been described elsewhere.[21,42,43] Briefly, a set of core-hole molecular orbitals (MOs) was obtained by the above DFT calculations. In the normal Auger transition, the final wave functions contain $(N-2)$ electrons with possible singlet and triplet spin multiplicities for the Auger final state since the initial state for the Auger decay was the doublet. Limited spin-symmetry-adapted CI calculations within the two-hole valence space were performed to determine the Auger final state wave functions. The Auger transition probability is approximated simply by atomic populations of valence orbitals on the excited atom while neglecting the term associated with the Auger electron. In the present study, Löwdin's population analysis is adopted. A similar formulation can be derived in the case of resonant Auger transitions in which case the wave functions describe $(N-1)$ electrons in the doublet Auger final state. There are two kinds of resonant Auger transitions: participant Auger, in which the excited electron participates in the Auger process, and spectator Auger, in which the excited electron stays in the excited orbital. Limited spin-symmetry-adapted CI calculations within the one-hole valence space were performed for the participant Auger final-state wave functions, while on the other hand, CI calculations within the one-particle–two-hole valence space were performed for the spectator decay process.

The participant and spectator Auger transition intensities are estimated in a similar way as for the normal Auger transition. Furthermore, two types of Auger decay calculations can be performed by either treating the participant and spectator Auger decay channels separately or by introducing channel coupling through mixed CI calculations using participant and spectator wave functions, which we call a resonant Auger decay calculation. Comparing the results of these two procedures the importance of configuration mixing between participant and spectator wave functions can be assessed. We confirmed in preliminary calculations that the resonant Auger decay and the separated calculations for a water molecule resulted in very similar spectra. For simplicity we will thus only discuss results from the resonant Auger decay calculations in the present study.

Auger decay calculations were performed for each CHES MD simulation snapshot. The theoretical spectra were constructed by convolution of the line spectra using Gaussian functions with a fixed full width at half maximum (FWHM) of 1.0 eV for the normal Auger spectrum and 0.7 eV for the first resonant Auger spectra over the whole energy range; this is substantially broader than the vibrationally resolved experiment but was adopted since quantized vibrations are not included in the classical dynamics. The final spectra were obtained by summation of spectra at 1 fs time steps from a series of trajectories weighted by the lifetime decay ratio $\exp(-t/\tau)$ where τ is the lifetime of the core hole; in this case 4.1 fs was used.[44] The MOLYX package has been used to calculate both the normal and resonant Auger spectra.

III. EXPERIMENTAL PROCEDURE

The gas-phase water experiments were performed using the ambient pressure photoemission endstation at beamline 11.0.2 at the Advanced Light Source in Berkeley, CA. The endstation is equipped with a differentially pumped electrostatic lens system[45] that transfers the electrons from the beam-spot position (which is at background pressures of up to 7 Torr) to the entrance slit of a Specs Phoibos 150 hemispherical electron spectrometer, that is kept in high vacuum. Impurities in the distilled water were removed by repeated cycles of freezing, pumping, and melting prior to leaking into the experimental chamber. The H_2O gas-phase pressure was kept at 0.7 Torr during the experiments. Both the photon resolution and the analyzer resolution were kept below 150 meV, resulting in a total resolution of about 200 meV.

IV. RESULTS AND DISCUSSION

A. Influence of CHES MD simulations

To exemplify the influence of the CHES MD simulations we show the time evolution of the normal and first resonant Auger spectra in Fig. 1 together with the trajectories of the CHES MD simulations during 20 fs. Gaussian functions with a FWHM of 1.0 eV were used to convolute the line spectra. The initial structure for both cases was the optimized ground-state geometry and the initial velocities were set to zero. The two different trajectories reflect the features of the core-excited state potentials. In the case of the normal Auger decay the bending mode is excited, but the change in the shape of the spectra due to the time evolution is not so large except for the region of 490–505 eV. Mitani *et al.* have computed the normal Auger spectrum of gas-phase water previously.[21] That spectrum corresponds to the spectrum at 0 fs in the present study. Although the CHES dynamics was not included in the earlier work, the obtained spectrum is very similar to the summed spectrum in the present work due to the minor structural changes obtained in the CHES MD simulations for this state.

Contrary to the normal Auger spectrum, the resonant Auger spectrum for the first core-excited state is sensitive to the CHES MD simulation. Note that the excitation energy is 533.0 eV. The first core-excited state, $O(1s) \rightarrow 4a_1$ excitation, is a well-known dissociative state.[6,7] According to the $Z+1$ approximation, the core-excited H_2O molecule corresponds to H_2F which is unstable to the dissociation to HF +H. In our CHES MD simulation, the two hydrogen atoms initially move symmetrically away from the oxygen atom, followed by one hydrogen returning to the oxygen and the other dissociating leading to bond scission into OH+H. This dynamics is reflected in the Auger spectrum, such that all peaks of the spectator Auger are shifted to higher kinetic

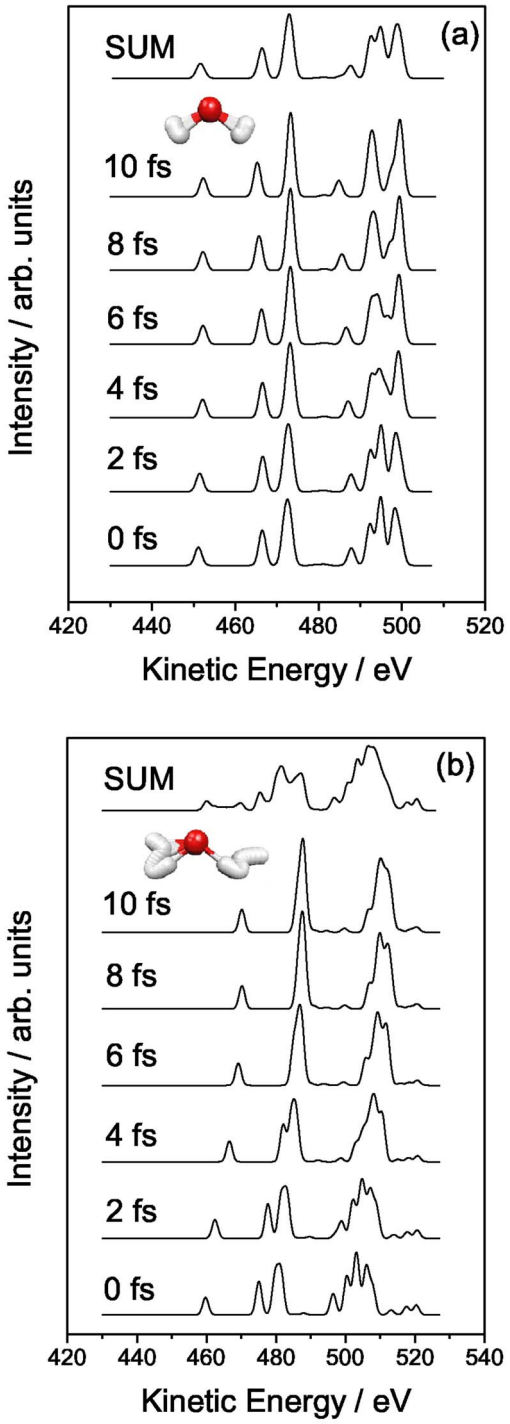

FIG. 1. (Color online) Time propagation of the Auger spectra by CHES MD simulations. Summed weighted spectra and a trajectory of this simulation during 20 fs are also shown. Gaussian functions with a FWHM of 1.0 eV were used to convolute the line spectra. The initial geometry is the ground-state equilibrium structure. (a) Normal Auger decay. (b) First resonant Auger decay. Excitation energy is 533.0 eV.

energy. On the other hand, peaks of the participant Auger are not as strongly affected. In summary, the normal Auger spectrum of water is insensitive to the CHES MD simulation, while on the other hand, the first resonant Auger spectrum is sensitive because of the excitation of the local OH stretching mode, which directly influences the chemical bond in the molecule.

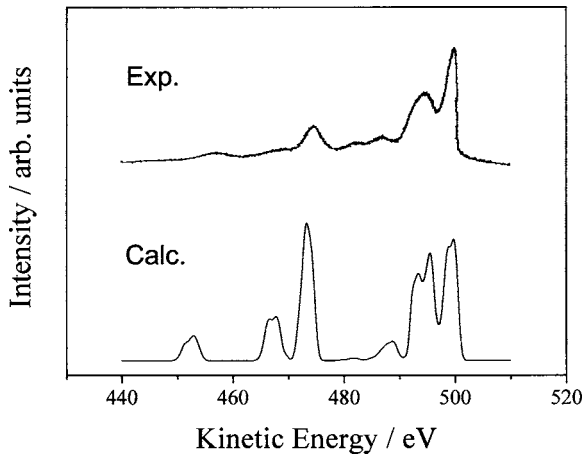

FIG. 2. Comparison of the experimental normal Auger spectrum of water (upper) to a calculated spectrum (bottom). The experimental spectrum is taken from Moddeman *et al.* (Ref. 46). The calculated spectrum is the sum of 60 spectra with different initial geometries for the CHES MD simulations.

B. Dynamical effects in the ground state

In the previous section, the initial geometry of H_2O was fixed at the equilibrium geometry of the ground state. However, a molecule in the ground state vibrates even at 0 K due to the zero-point energy. In order to include the effect of other instantaneous geometrical configurations in the ground state, 60 initial structures were picked up from MD simulations of the ground state. Auger decay spectra with CHES MD simulations starting from each initial geometry were obtained in the same way as in the previous section except for the initial velocities, which were set up to correspond to one of the ground-state normal modes, and summed spectra were made with equal weight for each spectrum. The results for the normal Auger spectrum are shown in Fig. 2 together with the experiment.[46] In comparison with the fixed ground-state geometry [previous section and Fig. 1(a)] some peaks become broader due to the dynamical effect of the nuclear motion. This effect is larger than the numerical error for the spectral resolution due to the large time step used in the MD simulation. The agreement with the experimental spectrum is nice except for the relative intensity of the peak at 472 eV. A similar analysis for the resonant Auger spectra of the first excited state reveals that the specific feature around 510 eV, associated with ultrafast dissociation,[7] does not show sufficient intensity in the simulations. In order to simulate this state more correctly, a special sampling procedure was used, as described in the following section.

C. Ultrafast dissociation of water: $O(1s) \rightarrow 4a_1$ excitation

Before displaying resonant Auger spectra for the $O(1s) \rightarrow 4a_1$ excitation, we discuss the potential-energy surfaces of water in the ground and first core-excited states shown in Fig. 3. The energy is relative to the ground-state equilibrium geometry and plotted as a function of OH distances for the electronic ground state (a) and the first core-excited state (b). Note that the HOH angle is fixed to 104.48 deg, that is the equilibrium geometry in the ground state. The ground state is bound with an OH bond length of

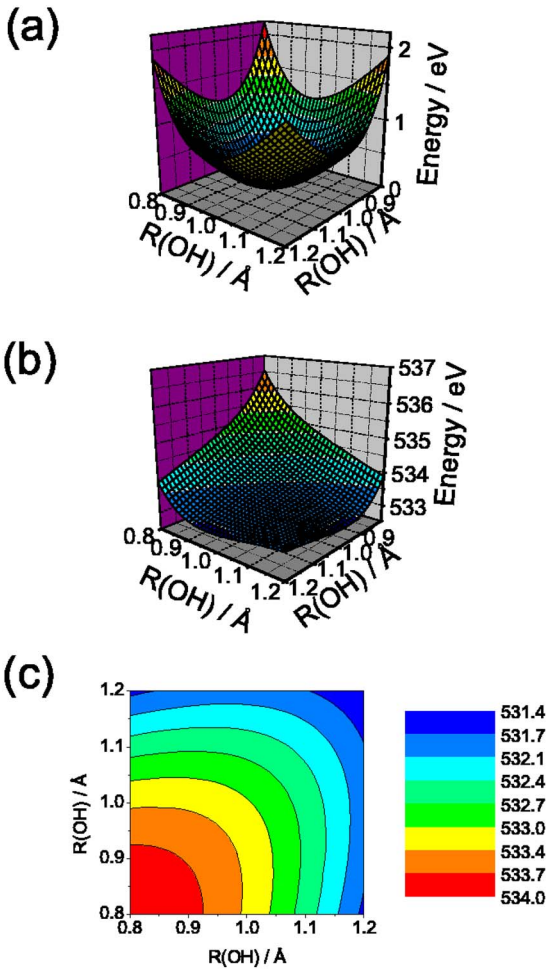

FIG. 3. (Color online) Potential-energy surfaces of water. Angle HOH is fixed to 104.6 deg. (a) The ground state and (b) the first resonant core-excited state. (c) Energy difference between the ground and first resonant core-excited states.

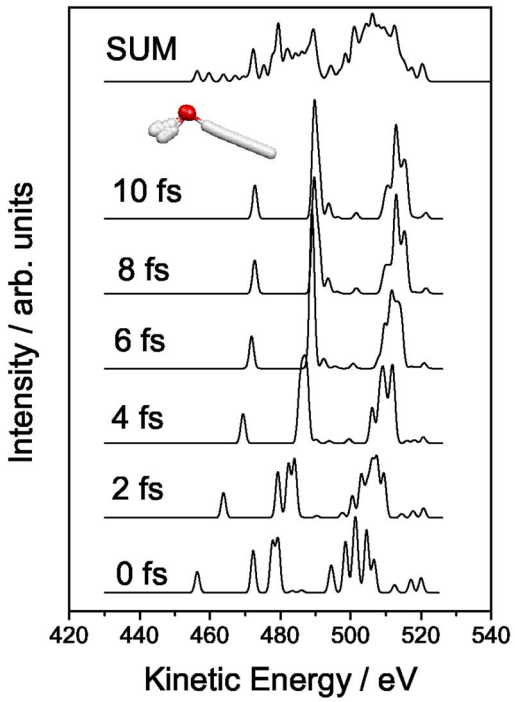

FIG. 4. (Color online) Time propagation of the Auger spectra by the CHES MD simulations for the first resonant Auger decay. Gaussian functions with a FWHM of 1.0 eV were used to convolute the line spectra. Note that the initial geometries are different compared with Fig. 1(b). Summed spectra with lifetime ratio and a trajectory of this simulation during 20 fs are also shown. Excitation energy is 533.96 eV.

ca. 0.98 Å, while the first excited state is dissociative to OH+H. The difference between the potential-energy surfaces, shown in Fig. 3(c), depends strongly on the geometry. At the equilibrium geometry, the excitation energy is only ca. 533.0 eV, which is fairly different from the peak position of the experimental x-ray-absorption spectra, 533.96 eV, due to the Franck-Condon factors between the ground and first core-excited states. Furthermore, Hjelte *et al.* have reported resonant Auger spectra changing the excitation energy using narrow bandwidth excitation.[7] The sampling scheme introduced in the last section is insufficient to reproduce such detuned spectra theoretically because of the limited geometrical variations probed by the classical vibrational dynamics. This leads to too-low excitation energies and a too-limited energy range. Simulations including quantum effects,[47] however, show a significant broadening of the vibrational distribution over that of the classical dynamics. In the present case this would imply a wider range of initial geometries and consequently a broader energy range. How can we access this higher excitation energy region?

If we use the ground-state equilibrium structure and assume vibrations to provide initial velocities, the selection of the velocity vectors becomes arbitrary. Instead, we choose to change the initial structure for the CHES MD simulations, i.e., probing only part of the vibrational distribution which effectively corresponds to creating a localized wave packet on the upper potential surface through narrow bandwidth excitation. For the initial geometries, more than a hundred points were sampled. The initial velocities of the CHES MD simulations were set to zero. In order to simulate the experimental spectra for a given excitation energy E_0, the spectra from each geometry were summed with a Gaussian weight,[48]

$$I(E) = \exp\left[-\frac{1}{2} \frac{(E - E_0)^2}{(\Gamma_G / c)^2} \right], \tag{1}$$

where E is the excitation energy for the sampled geometry, Γ_G is FWHM of the excitation energy, and $c \equiv 2\sqrt{\ln 4} \simeq 2.355$. For comparison with experiments (see Experimental procedure section and Ref. 7) we used 140 meV for the FWHM.

In Fig. 4 Auger spectra and trajectories from the CHES MD simulation are shown for a *single* initial geometry corresponding to 533.96 eV excitation energy. Note that Gaussian functions with a FWHM of 1.0 eV were used to convolute the line spectra. From Fig. 3(c) we associate 533.96 eV to the sampling in the shorter bond-length region. It is obvious that one of the hydrogen atoms migrates faster than in the CHES MD simulation for the ground-state equilibrium geometry [Fig. 1(b) and Sec. IV A]. As a consequence of the accelerated dynamics, peak shifts to higher kinetic energies occur on a shorter time scale, and the summed spectra gain intensity around 512 eV. The enhancement of this spectral

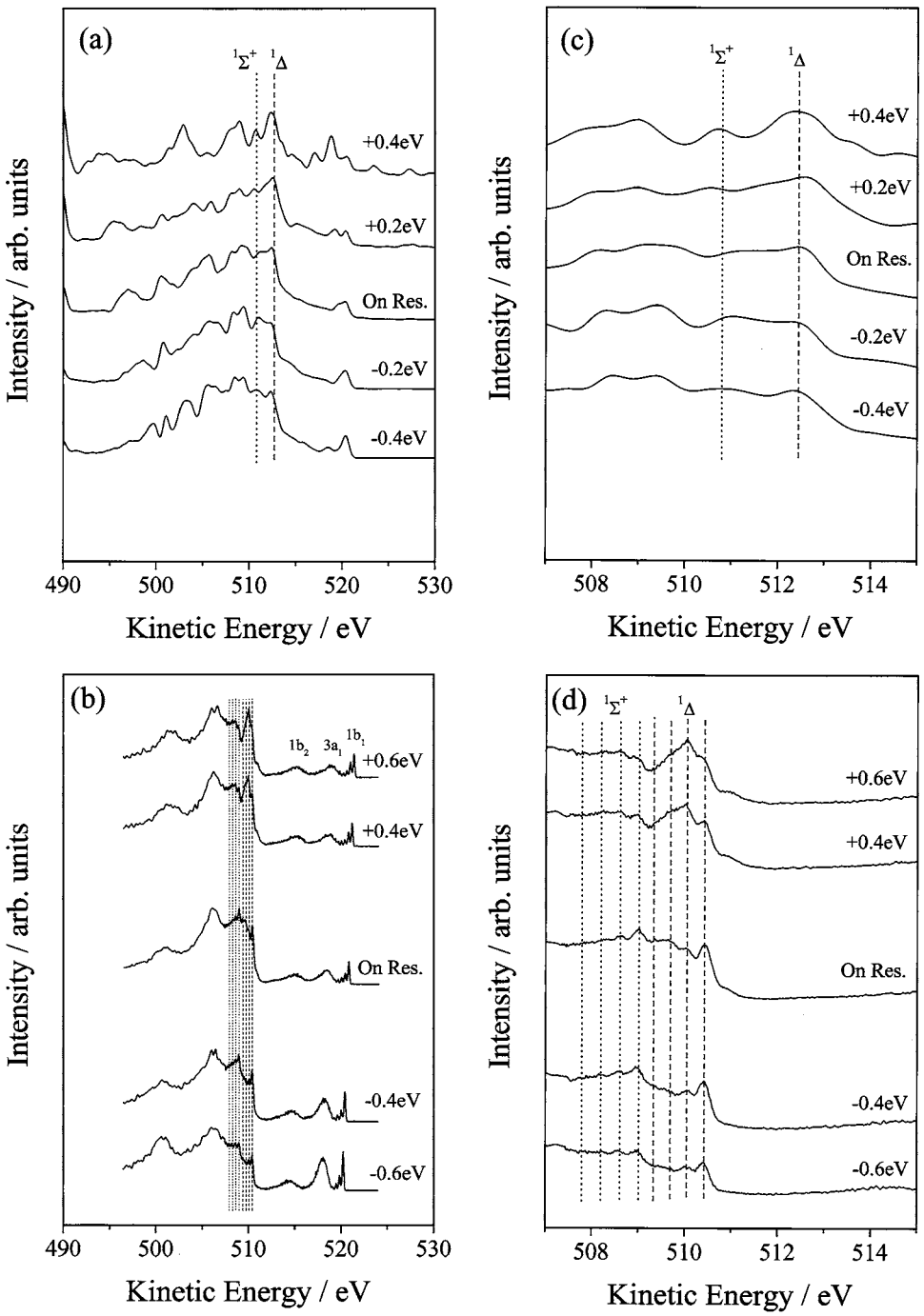

FIG. 5. Resonant Auger spectra of water following $O(1s) \rightarrow 4a_1$ excitation. The detuning is relative to the center of the $O(1s) \rightarrow 4a_1$ absorption resonance (533.96 eV). Peak assignments are also shown. (a) Calculated spectra. (b) Experimental spectra. (c) An enlarged view of (a). (d) An enlarged view of (b).

feature, assigned to the fragment Auger originating from OH^+,[7] can thus be captured by the excited-state dynamics in this procedure. The effect of the dynamics for different excitation energies is shown in Fig. 5. To avoid peak broadening due to summation of many spectra, Gaussian functions with a FWHM of 0.7 eV were used to convolute the line spectra for each CHES MD simulation. Using the described procedure we obtain Auger spectra for a different detuning relative to 533.96 eV in Fig. 5(a) [magnified in Fig. 5(c)]. For comparison, the experimental spectra with the same kinetic-energy range are shown in Fig. 5(b) [magnified in Fig. 5(d)]. In the experimental spectra, the region around 508–512 eV shows a vibrational manifold that is similar to the experimental results in Ref. 7. The guidelines in the figure underline the vibrational fine structure of the final states, assigned to $^1\Delta$ and $^1\Sigma^+$ states of OH as a fragment by Hjelte *et al.* Our simulations are performed using classical mechanics, so we cannot reproduce the vibrational structure which is due to quantum-mechanical effects such as the Franck-Condon factor between the Auger final state and the first core-excited state. What we can observe, however, is the trend of the vibrationally unresolved, i.e., integrated, intensity. Inspecting the enlarged view of the theoretical spectra in Fig. 5(c), we find that the relative intensity of the states around 510 eV increases linearly with the excitation energy, consistent with the experimental observations. The increase of the spectral intensity here is directly related to the excited-state dynamics, such that excitation energy detuning above

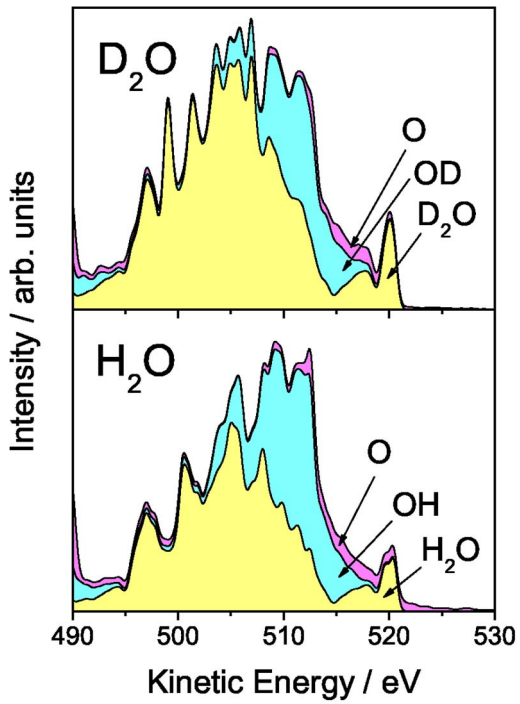

FIG. 6. (Color online) A comparison between calculated resonant Auger spectra of H_2O and D_2O after $O(1s) \rightarrow 4a_1$ core excitation. Contributions from fragments are also shown.

the resonance, corresponding to ground-state sampling in a shorter bond-length region, is associated with a faster dynamics and consequently larger intensity in the higher kinetic-energy region of about 510 eV. A more quantitative description of the final-state fragmentation can thus be obtained as is further described in the following.

Isotope effects for H_2O/D_2O on the first resonant Auger spectra of water have been observed experimentally by Hjelte *et al.* They have proposed that the decrease of the intensity from the fragment Auger for D_2O corresponds to late dynamics due to the increased mass. We have simulated the Auger spectra also for D_2O and the results are shown in Fig. 6; the faster dissociation of H_2O compared with D_2O is easily seen. The difference in the dynamical effect is reflected in the Auger spectra, i.e., the intensity around 510 eV

TABLE I. OH bond-length elongation (in Å) within a core-hole lifetime of 4.1 fs.

Excitation energy (eV)	H_2O (Å)	D_2O (Å)
533.0	1.181	1.111
533.2	1.203	1.122
533.56	1.553	1.285
533.76	1.658	1.330
533.96 (On res.)	1.789	1.396
534.16	1.960	1.487
534.36	2.108	1.559

decreases in the D_2O Auger spectrum due to the late dissociation. In order to understand the effect of fast dissociation, we analyze our simulations further.

Firstly, we can estimate the OH bond elongation within the $O(1s)$ core-hole lifetime. The OH bond length at 4.1 fs was obtained from the CHES MD trajectories for each sampled geometry, and summed with the Gaussian weight described above for each excitation energy E_0. The results are summarized in Table I. With increasing excitation energy, we find that the OH bond length after 4.1 fs gradually increases, suggesting that the dissociation of the OH bond is getting faster as the excitation energy is increased. The isotope effect is clearly seen, i.e., the OH bond of H_2O elongates faster than D_2O due to the smaller mass of hydrogen.

Secondly, the above OH bond elongation is related to the initial geometry of the CHES MD simulations. Three contour maps of the OH bond length after 4.1 fs propagation as a function of different initial geometries in the CHES MD simulation are shown in Fig. 7. Note that only the longer of the two OH bonds is shown. The maps are very similar even if the bending angles are different, suggesting that the bending is not so important for dissociation. Initial structures with asymmetric OH bond lengths contribute more to the OH bond elongation, indicating that the excitation of the antisymmetric stretching mode is important for this dissociation channel.

Thirdly, we can estimate the product ratio $H_2O:OH:O$ from each trajectory where we take an OH bond as dissociated if that bond length becomes larger than 1.5 Å, which is

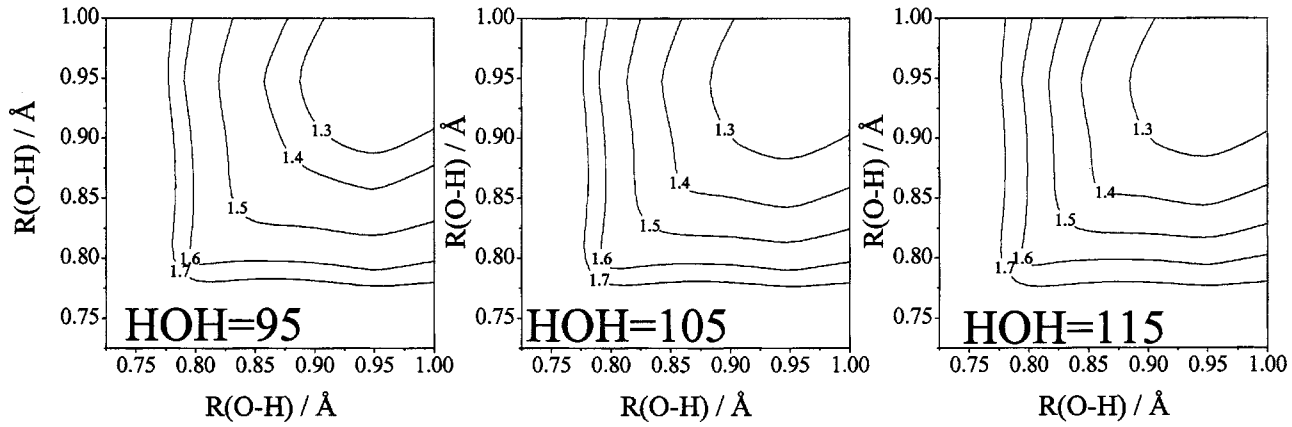

FIG. 7. Bond-length contour map showing the dependence on the initial geometry of the CHES MD simulations. Only the longer OH bond length during the core-hole lifetime (4.1 fs) is indicated.

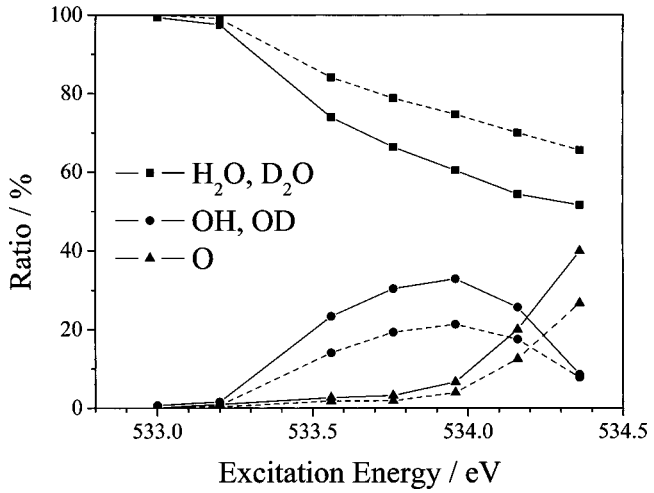

FIG. 8. Fragment ratio depending on the excitation energy. Solid and dashed lines indicated, respectively, H_2O and D_2O and their products.

longer than 1.5 times the ground-state equilibrium bond length. We confirmed that an oscillating OH bond for most CHES MD simulations does not exceed the above threshold bond length. Thus an OH bond longer than 1.5 Å can be regarded as broken. The results are shown in Fig. 8. At an excitation energy of 533.0 eV, most products are H_2O. Increasing the excitation energy, the fraction of undissociated H_2O gradually decreases and the amounts of OH and O increase. The contribution to the Auger spectra from atomic oxygen as a dissociation product has not been discussed earlier. The amount of OH becomes maximum at an $O(1s) \rightarrow 4a_1$ excitation energy of 533.96 eV. After that, the OH fraction gradually decreases while the amount of O (atom) increases. In the case of D_2O, the D_2O ratio is substantially higher than H_2O due to the slower movement of the heavier isotope. Using the information from Fig. 8, we can decompose the calculated Auger spectra into contributions from each product. The results are also shown in Fig. 6. Hjelte *et al.* have interpreted their experimental Auger spectra as the sum of the H_2O spectator and participant Auger plus the OH fragment Auger. In our model calculations, we reproduce the increase of the intensity around 512 eV due to the fragment Auger of OH. Furthermore, from our simulations we found that resonant Auger spectra partially include atomic Auger decay. The fraction of atomic Auger decay increases with increasing excitation energy. However, our estimation of the fraction of O may be too large at +0.4 eV due to the approximate sampling scheme for initial conditions of MD simulations. Improving these initial conditions will be the subject of further work.

V. SUMMARY

In the present paper, we discussed the theoretical normal and resonant Auger spectra using CHES MD simulations in combination with CI calculations using DFT Kohn-Sham orbitals. Save for the final-state vibrational structure, we can reproduce not only the normal experimental Auger spectrum of water, but also the first resonant Auger spectrum. We found that the normal Auger spectrum of water is insensitive to the core–hole-induced dynamics, while the first resonant Auger spectrum is sensitive because of the excitation of the OH stretching local mode. In the analysis of the first resonant Auger spectrum, we found that the experimental spectra can be interpreted as the mixed spectra of intact H_2O with OH and O fragments. The amount of fragments increases with the excitation energy, which affects the calculated spectra and the experimental trends. Our procedure can be applied to polyatomic molecules, or more complex molecular systems, for example, in the modeling of condensed phase. Although our model for the Auger decay process is a two-step model, the overall spectral trend under an Auger resonant Raman condition could still be reproduced.

ACKNOWLEDGMENTS

The authors thank Professor V. Carravetta for helpful discussions and comments. Support from the Foundation for Strategic Research and the Swedish Science Council is gratefully acknowledged. The ALS-MES beamline 11.0.2 is supported by the Director, Office of Science, Office of Basic Energy Sciences, Division of Chemical Sciences, Geosciences, and Biosciences and Materials Sciences Division of the U.S. Department of Energy at the Lawrence Berkeley National Laboratory under Contract No. DE-AC03-76SF00098. Part of one of the author's (D.N.) work is supported by the Wenner-Gren Foundation.

[1] W. Mehlhorn, J. Electron Spectrosc. Relat. Phenom. **93**, 1 (1998).
[2] M. N. Piancastelli, J. Electron Spectrosc. Relat. Phenom. **107**, 1 (2000).
[3] P. Porin and I. Nenner, Phys. Rev. Lett. **56**, 1913 (1986).
[4] O. Björneholm, S. Sundin, S. Svensson, R. R. T. Marinho, A. Naves de Brito, F. Gel'mukhanov, and H. Ågren, Phys. Rev. Lett. **79**, 3150 (1997).
[5] H. Aksela, S. Aksela, M. Ala-Korpela, O. P. Sairanen, M. Hotokka, G. M. Bancroft, K. H. Tan, and J. Talkki, Phys. Rev. A **41**, 6000 (1990).
[6] A. Naves de Brito, R. Feifel, A. Mocellin, A. B. Machado, S. Sundin, I. Hjelte, S. L. Sorensen, and O. Björneholm, Chem. Phys. Lett. **309**, 377 (1999).
[7] I. Hjelte, M. N. Piancastelli, R. F. Fink *et al.*, Chem. Phys. Lett. **334**, 151 (2001).
[8] B. Brena, D. Nordlund, M. Odelius, H. Ogasawara, A. Nilsson, and L. G. M. Pettersson, Phys. Rev. Lett. **93**, 148302 (2004).
[9] M. Odelius, H. Ogasawara, D. Nordlund *et al.*, Phys. Rev. Lett. **94**, 227401 (2005).
[10] M. Alagia, R. Richter, S. Stranges *et al.*, Phys. Rev. A **71**, 012506 (2005).
[11] I. Hjelte, L. Karlsson, S. Svensson *et al.*, J. Chem. Phys. **122**, 084306 (2005).
[12] M. N. Piancastelli, R. Sankari, S. Sorensen, A. De Fanis, H. Yoshida, M. Kitajima, H. Tanaka, and K. Ueda, Phys. Rev. A **71**, 010703 (2005).
[13] A. Nambu, E. Kobayshi, M. Mori, K. K. Okudaira, N. Ueno, and K. Mase, Surf. Sci. **593**, 269 (2005).
[14] B. Schimmelpfennig, B. M. Nestmann, and S. D. Peyerimhoff, J. Electron Spectrosc. Relat. Phenom. **74**, 173 (1995).
[15] B. Schimmelpfennig and S. D. Peyerimhoff, Chem. Phys. Lett. **253**, 377 (1996).
[16] S. K. Botting and R. R. Lucchese, Phys. Rev. A **56**, 3666 (1997).
[17] R. Fink, J. Electron Spectrosc. Relat. Phenom. **76**, 295 (1995).
[18] R. Fink, J. Chem. Phys. **106**, 4038 (1997).
[19] R. Fink, S. L. Sorensen, A. Naves de Brito, A. Ausmees, and S. Svensson, J. Chem. Phys. **112**, 6666 (2000).
[20] U. Hergenhahn, A. Rudel, A. M. Bradshaw, R. F. Fink, and A. T. Wen, Chem. Phys. **289**, 57 (2003).
[21] M. Mitani, O. Takahashi, K. Saito, and S. Iwata, J. Electron Spectrosc. Relat. Phenom. **128**, 103 (2003).
[22] T. Otsuka, S. Koizumi, K. Endo, and D. P. Chong, J. Surf. Anal. **9**, 467 (2002).
[23] T. Otsuka, S. Koizumi, K. Endo, and D. P. Chong, J. Mol. Struct.: THEOCHEM **619**, 241 (2002).

[24] T. Otsuka, D. P. Chong, J. Maki, H. Kawabe, and K. Endo, Chem. Phys. Lett. **352**, 511 (2002).
[25] F. Gel'mukhanov and H. Ågren, Phys. Rev. A **54**, 379 (1996).
[26] F. Gel'mukhanov and H. Ågren, Phys. Rev. A **54**, 3960 (1996).
[27] L. S. Cederbaum and F. Tarantelli, J. Chem. Phys. **98**, 9691 (1993).
[28] Z. W. Gortel, R. Teshima, and D. Menzel, Phys. Rev. A **58**, 1225 (1998).
[29] Z. W. Gortel and D. Menzel, Phys. Rev. A **58**, 3699 (1998).
[30] P. Salek, F. Gel'mukhanov, and H. Ågren, Phys. Rev. A **59**, 1147 (1999).
[31] F. Tarantelli, A. Sgamellotti, and L. S. Cederbaum, J. Electron Spectrosc. Relat. Phenom. **68**, 297 (1994).
[32] D. Minelli, F. Tarantelli, A. Sgamellotti, and L. S. Cederbaum, J. Electron Spectrosc. Relat. Phenom. **74**, 1 (1995).
[33] F. Tarantelli, L. S. Cederbaum, and A. Sgamellotti, J. Electron Spectrosc. Relat. Phenom. **76**, 47 (1995).
[34] S. Tanaka, Y. Kayanuma, and K. Ueda, Phys. Rev. A **57**, 3437 (1998).
[35] L. Triguero, L. G. M. Pettersson, and H. Ågren, Phys. Rev. B **58**, 8097 (1998).
[36] C. Kolczewski, R. Püttner, O. Plashkevych *et al.*, J. Chem. Phys. **115**, 6426 (2001).
[37] O. Takahashi and L. G. M. Pettersson, J. Chem. Phys. **121**, 10339 (2004).
[38] W. Kutzelnigg, U. Fleischer, and M. Schindler, *NMR Basic Principles and Progress* (Springer-Verlag, Heidelberg, 1990).
[39] J. P. Perdew and Y. Wang, Phys. Rev. B **33**, 8800 (1986).
[40] J. P. Perdew and Y. Wang, Phys. Rev. B **45**, 13244 (1992).
[41] K. Hermann, L. G. M. Pettersson, M. E. Casida *et al.*, STOBE-DEMON version 2.0 (2004).
[42] O. Takahashi, M. Mitani, M. Joyabu, K. Saito, and S. Iwata, J. Electron Spectrosc. Relat. Phenom. **120**, 137 (2001).
[43] O. Takahashi, M. Joyabu, M. Mitani, K. Saito, and S. Iwata, J. Comput. Chem. **24**, 1329 (2003).
[44] R. Sankari, M. Ehara, H. Nakatsuji, Y. Senba, K. Hosokawa, H. Yoshida, A. De Fanis, Y. Tamenori, S. Aksela, and K. Ueda, Chem. Phys. Lett. **380**, 647 (2003).
[45] D. Frank Ogletree, H. Bluhm, G. Lebedev, C. Fadley, Z. Hussain, and M. Salmeron, Rev. Sci. Instrum. **73**, 3872 (2002).
[46] W. E. Moddeman, T. A. Carlson, M. O. Krause, and B. P. Pullen, J. Chem. Phys. **55**, 2317 (1971).
[47] H. A. Sterne and B. J. Berne, J. Chem. Phys. **115**, 7622 (2001).
[48] J. Stöhr, *NEXAFS Spectroscopy* (Springer, Berlin, 1992).